

# TOKAMARK: A Comprehensive Benchmark for MAST Tokamak Plasma Models

Cécile Rousseau  
IBM Research Europe  
Dublin, Ireland  
rousseau.cecile@ibm.com

Nicola C. Amorisco  
UK Atomic Energy Authority  
Abingdon, UK  
nicola.amorisco@ukaea.uk

Andrea Loreti  
UK Atomic Energy Authority  
Abingdon, UK  
andrea.loreti@ukaea.uk

Adriano Agnello  
STFC Hartree Centre  
Daresbury, UK  
adriano.agnello@stfc.ac.uk

Robert Akers  
UK Atomic Energy Authority  
Abingdon, UK  
rob.akers@ukaea.uk

Samuel Jackson  
UK Atomic Energy Authority  
Abingdon, UK  
samuel.jackson@ukaea.uk

Tobia Boschi  
IBM Research Europe  
Dublin, Ireland  
tobia.boschi@ibm.com

Eszter Székely  
UK Atomic Energy Authority  
Abingdon, UK  
eszter.szekely@ukaea.uk

Stanislas Pamela  
UK Atomic Energy Authority  
Abingdon, UK  
Stanislas.Pamela@ukaea.uk

Juan Bernabe Moreno  
IBM Research Europe  
Dublin, Ireland  
juan.bernabe-moreno@ibm.com

Mykhaylo Zayats  
IBM Research Europe  
Dublin, Ireland  
mykhaylo.zayats1@ibm.com

Rodrigo H. Ordonez-Hurtado  
IBM Research Europe  
Dublin, Ireland  
rodrigo.ordonez.hurtado@ibm.com

George K. Holt  
STFC Hartree Centre  
Daresbury, UK  
george.holt@stfc.ac.uk

Alexander Whittle  
UK Atomic Energy Authority  
Abingdon, UK  
alexander.whittle@ukaea.uk

Alessandra Pascale  
IBM Research Europe  
Dublin, Ireland  
apascale@ie.ibm.com

Sue Thorne  
STFC Hartree Centre  
Daresbury, UK  
sue.thorne@stfc.ac.uk

## Abstract

Development and operation of commercially viable fusion energy reactors such as tokamaks require accurate predictions of plasma dynamics from sparse, noisy, and incomplete sensors readings. The complexity of the underlying physics and the heterogeneity of experimental data pose formidable challenges for conventional numerical methods, while simultaneously highlights the promise of modern data-native AI approaches. A major obstacle in realizing this potential is, however, the lack of curated, openly available datasets and standardized benchmarks. Existing fusion datasets are scarce, fragmented across institutions, facility-specific, and inconsistently annotated, which limits reproducibility and prevents a fair and scalable comparison of AI approaches. In this paper, we introduce **TOKAMARK**, a structured benchmark to evaluate AI models on real experimental data collected from the Mega Ampere Spherical Tokamak (MAST). **TOKAMARK** provides a comprehensive suite of tools designed to (i) unify access to multi-modal heterogeneous fusion data (ii) harmonize formats, metadata, temporal alignment and evaluation protocols to enable consistent cross-model and cross-task comparisons. The benchmark includes a curated list of 14 tasks spanning a range of physical mechanisms, exploiting

a variety of diagnostics and covering multiple target use cases. A baseline model is provided to facilitate transparent comparison and validation within a unified framework. By establishing a unified benchmark for both the fusion and AI-for-science communities, **TOKAMARK** aims to accelerate progress in data-driven plasma AI modeling, contributing to the broader goal of achieving sustainable and stable fusion energy. The benchmark, documentation, and tooling will be fully open sourced upon acceptance to encourage community adoption and contribution.

## CCS Concepts

- **Hardware** → **Renewable energy**; • **Software and its engineering** → **Software libraries and repositories**; **Open source model**; • **Information systems** → **Extraction, transformation and loading**; **Evaluation of retrieval results**.

## Keywords

AI for science, Fusion benchmark, Data-driven plasma modeling, Multi-modal learning, MAST tokamak

## 1 Introduction

Nuclear fusion power is being explored as a potential long-term energy source with a unique combination of benefits. It offers the prospect of a carbon-neutral energy supply with abundant fuel and significant safety advantages over nuclear fission. However commercially viable fusion demands stable, sustained reactions that produce more power than the reactor consumes – a goal made difficult by the extreme physical conditions of thermonuclear confinement under which fusion must operate [3].

Fusion reactors such as tokamaks aim to reproduce on Earth the same process that powers the Sun, confining a plasma hotter than 100 million degrees Celsius using strong rapidly evolving magnetic fields because no material surface can survive direct contact with such plasma. This environment forces all measurements to be non-invasive and indirect, only partially inferring plasma state while the underlying dynamics evolve on microsecond-to-millisecond timescales. In this work, we dedicate our attention to the problem of modeling fusion plasma dynamics in tokamaks – one of the central challenges in fusion research. This problem encompasses a wide set of predictive tasks, including plasma shape and equilibrium inference, transport and profile evolution, and forecasting of MHD activity and disruptions.

### 1.1 AI for fusion plasma modeling

Traditional tokamak plasma modeling approaches rely either on first-principles, physics-driven solvers or on complex system identification pipelines. Although the governing physics is well understood, it is expressed through complex nonlinear partial differential equations whose key parameters are often unmeasured, only partially observable, or must be inferred indirectly from diagnostics. As a result, classical methods tend to be computationally intensive, brittle across operating regimes, and difficult to apply in real time. These challenges are further exacerbated by the nature of the experimental data itself, which reflects the extreme environment and sensing limitations of tokamak operation.

Tokamaks deploy a broad suite of heterogeneous diagnostics – magnetics, optical and X-ray emission, microwave interferometry, and more – mounted on or behind the reactor walls and engineered to withstand heat, radiation, and electromagnetic stress. These sensors operate at widely different sampling rates, spatial resolutions, and noise characteristics producing data that is inherently heterogeneous, incomplete, multi-rate and noisy.

Together, the complexity of the underlying physics and the heterogeneity of the data create an opportunity where modern AI methods can provide significant advantages. Data-driven models are well suited to fusing multi-modal diagnostics, learning latent plasma representations, and capturing nonlinear, multi-scale temporal behavior. Unlike traditional solvers, AI models can operate directly on raw measurements, handle missing or asynchronous data, and produce accurate and efficient surrogates. This positions AI as a promising complement to physics-based modeling for understanding, predicting, and ultimately controlling fusion plasma.

Previous work applying AI to fusion plasma problems have demonstrated promising results across variety of narrowly defined

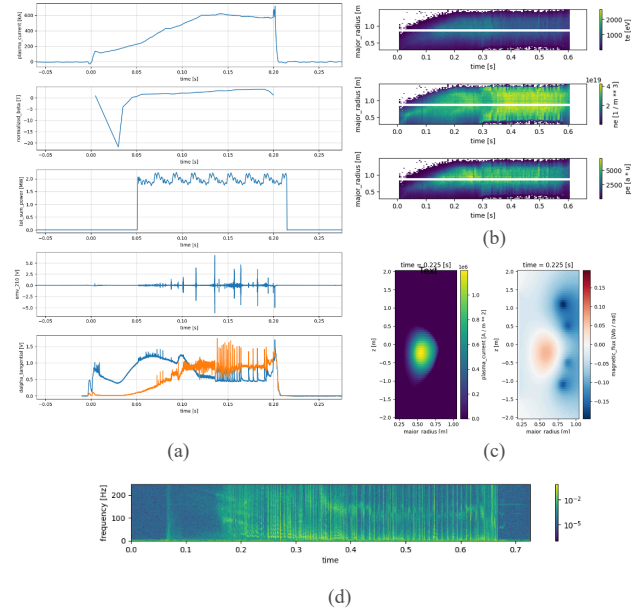


**Figure 1: Examples of multi-modal signals from the FAIR-MAST dataset: a) Time series of plasma current, beta normal, NBI power, mirnov coils, and  $D_{\alpha}$  signals; b) Thomson scattering profiles of electron temperature, density, and pressure; c) maps of plasma current and magnetic flux; d) profile of the mirnov coils spectrogram.**

tasks, ranging from plasma shape reconstruction and profile forecasting to actuator optimization and disruptions prediction. However, most of those efforts use bespoke pipelines tailored to a small set of diagnostics, single device and single scientific objective, relying heavily on task-specific feature engineering and handcrafted labeling procedures. While successful within their respective scopes, these approaches typically optimize models for individual tasks and limit reuse across the experimental lifecycle. Much more work is needed to move beyond isolated point solutions toward broad, interoperable models capable of understanding fusion plasmas in a comprehensive way.

Inspired by the success of Foundation Models (FM) in language and vision, there is a growing expectation that analogous models trained on large corpora of tokamak data could learn rich, transferable plasma representations [1]. These models aim to internalize latent physical structure directly from data, serving as data-driven analogs of first-principles knowledge that can support a wide range of downstream tasks. Although still in early stages, this paradigm suggests a path toward generalist AI systems for fusion that complement physics-based modeling and reduce the need for handcrafted pipelines [1].

Progress toward either specialized or generalist plasma models is hampered by the absence of open, standardized benchmarks. Fusion datasets remain fragmented across institutions, locked behind proprietary interfaces, or stored in domain-specific formats that are difficult for Machine Learning researchers to access or interpret [9]. Without unified task definitions, metrics, or evaluation protocols, it becomes impossible to provide fair comparison of methods

and to measure progress systematically. A benchmark is therefore needed to frame the plasma modeling problems in a broader and more structured way, enabling cross-comparison across algorithms, reproducibility across labs, and accessibility for researchers both inside and outside the fusion community.

At the same time, fusion diagnostic data provides unique set of challenge going beyond those found in standard datasets from more established areas of AI. The data is inherently multi-modal, multi-rate, and multi-dimensional, with wide variations in signal quality, noise characteristics, and information content (see Figure 1 for an illustrative example). Many diagnostics operate asynchronously, contain gaps, or suffer partial failures; others produce high-dimensional structured outputs such as flux maps or spectrograms. This complexity demands dedicated modeling approaches that can handle missing data, fuse heterogeneous signals, different modalities, and reason across fast and slow timescales – capabilities that are difficult to stress-test without a standardized benchmark.

Taken together, these factors create a clear need for a comprehensive benchmark suite that defines common tasks, standardizes evaluation, and provides open access to representative fusion data. Establishing such a benchmark is essential for accelerating research, enabling fair comparison of models, and ultimately advancing data-driven plasma understanding and control.

## 1.2 TOKAMARK Benchmark Overview

To fill the need of comprehensive fusion plasma benchmarks we introduce TOKAMARK the first large, open benchmark for evaluating AI models trained on *real* fusion diagnostics, built from recently released FAIR-MAST data [4, 5].

**Data.** To the best of our knowledge, FAIR-MAST is the only openly available dataset of real tokamak diagnostics. Recent releases [4, 5] curate a collection of real experiments and corresponding diagnostics measurements from MAST tokamak. From FAIR-MAST, we select 39 signals across heterogeneous modalities, harmonize metadata and build standardized loaders.

**Tasks.** For TOKAMARK we defined a diverse suite of 14 downstream tasks designed to probe core capabilities required of AI models for fusion plasmas: (i) representation learning from heterogeneous diagnostics; (ii) temporal reasoning across fast and slow timescales; (iii) robustness to incomplete state information; and (iv) generalization across operating regimes. Rather than optimizing for a single downstream objective, the tasks, organized into four groups, span a cascade of physical processes – from fast magnetic response to slower, transport-driven evolution and long-horizon precursors of MHD activity – while remaining closely aligned with routine experimental workflows. Wherever possible, tasks minimize reliance on expert-labeled targets, supporting self-supervised and weakly supervised formulations and enabling systematic evaluation of transferable plasma representations.

**Evaluation.** We introduce a hierarchical evaluation protocol aligned with the structure of FAIR-MAST and with scientific objectives. This hierarchy assesses both low-level prediction quality and high-level scientific meaning. For specialized models (single-task training), the hierarchy yields granular, signal-level diagnostics; for generalist models (FM-style pretraining across tasks), it provides modular comparisons across tasks and broad scientific objectives.

**Baseline.** Finally, we provide a strong yet accessible baseline: a *multi-branch convolutional encoder-decoder* architecture trained per each task that ingests heterogeneous inputs and predicts task-specific targets.

The following list summarizes our contributions:

- **Benchmark design.** We define 14 tasks organized into four groups, with a hierarchical evaluation protocol, standardized windowing and error metrics.
- **Data packaging.** We freeze a stable subset of FAIR-MAST, resolve schema inconsistencies, standardize metadata and units, and release it for reproducibility and long time compatibility.
- **Tools and API.** We provide a Python package for task-specific data loading, processing and batching, masking and alignment utilities, and evaluation logic, integrated with PyTorch stack.
- **Baseline models.** We release a multi-branch convolutional encoder-decoder baseline with reference configurations and training scripts, establishing reproducible baselines across all tasks [7] [8].

## 2 Preliminaries

To ground TOKAMARK benchmark in the reality of complex heterogeneous fusion data, we first introduce a signal taxonomy that organizes these measurements by function and modality, and allows us to provide a consistent vocabulary for describing inputs, targets, and tasks in the benchmark.

### 2.1 Data Taxonomy

MAST is a spherically-shaped tokamak located in Culham, Oxfordshire (UK) and was operated by UKAEA and EURATOM from 1999 to 2013 [2, 6, 10]. MAST and tokamaks in general operate in short experimental cycles known as *discharges* or *shots*. The length of those cycles depends on the device size and in the case of MAST they are typically lasting around 2–3 seconds. Over its operational lifetime, MAST produced more than 30,000 shots, with each shot containing diagnostic signals measuring various properties of the plasma, including the magnetic field, plasma temperature, shape parameters, applied heating etc.

Recent works [4, 5] have created an open dataset of diagnostic data from a subset of the history of MAST. The FAIR-MAST dataset contains 11,573 shots from the last five experimental campaigns on MAST. In this work we utilized a total of 39 signals from FAIR-MAST in the design of our benchmark tasks.

We organize all signals along several complementary axes, summarized in Table 1. First, we group signals by *category*, which encodes their physical semantics—that is, the physical quantities they represent and how they are used by MAST workflows. This information corresponds to the first two columns of Table 1. Note that the second column contains both individual signals and *subcategories*. These intermediate groupings are introduced for brevity: they consolidate multiple signals that are typically used together (at least within the proposed benchmark) and share the same structural and functional properties. For example, the *shape parameters* subcategory includes several attributes jointly describing plasma

**Table 1: Signals taxonomy for TOKAMARK.**

Category	Subcategory/Signals	Origin	Frequency	Modality
<b>Magnetics</b>	Flux loops, pickup coils; saddle coils	Sensor	5 kHz; 50 kHz	Profile
<b>Kinetics</b>	Thomson scattering; interferometer	Sensor	0.2 kHz; 4 kHz	Profile; time series
<b>Radiatives</b>	D <sub>alpha</sub> , soft X-ray	Sensor	50 kHz	Profile
<b>MHD Precursors</b>	Mirnov coils	Sensor	500 kHz	Profile
<b>Currents</b>	Poloidal Field Coil currents; Solenoid current, Plasma current	Sensor	4 kHz	Profile; Time series
<b>Voltages</b>	Poloidal Field Coil voltages	Actuator	4 kHz	Profile
<b>References</b>	Reference Plasma Current, Reference Plasma Density	Actuator	4 kHz	Time series
<b>Fueling</b>	NBI power, gas puffing	Actuator	4 kHz	Time series
<b>Equilibrium</b>	Shape parameters, $\beta$ metrics; plasma boundary; flux map	Derived	0.2 kHz	Time series; profile; video

geometry. A full list of the signals used in this work is provided in the appendix in Table 4.

Second, we distinguish signals by their *origin*. We define three classes: (i) **sensors**, corresponding to direct hardware measurements; (ii) **actuators**, representing controllable machine parameters used to steer plasma behavior; and (iii) **derived** signals, comprising quantities produced by reconstruction pipelines such as EFIT (e.g., shape parameters or flux maps).

The third axis is *frequency*, reflecting the wide range of sampling rates across diagnostics, and spanning from 0.2 kHz up to 500 kHz. Finally, the fourth axis is *modality*, describing the structural form of each signal: (i) **time series**, represented as 1D tensors (scalar value over time); (ii) **profiles**, represented as 2D tensors (vector over time); and (iii) **videos**, represented as 3D tensors (image over time). These latter two axes are particularly important for guiding the design of AI model architectures and loss functions.

## 2.2 Tasks Structural Taxonomy

The downstream tasks in TOKAMARK share a common structural formulation designed to reflect the online, window-based nature of plasma control and forecasting in tokamak experiments. Rather than operating on full-shot signals (as is often done in offline post-discharge analysis), our tasks are defined using **input window** and **output window** anchored at a reference time point.

Each task consists of one or more *input signals* and one or more *output signals* also referred to as targets. Inputs typically include both sensor signals (e.g., magnetics, radiatives, kinetics) and actuator signals (e.g., voltages, fueling), while outputs include either sensor signals or derived quantities like equilibrium reconstructions.

The alignment between the input and output windows naturally induces several families of modeling objectives:

- **Reconstruction.** Given a set of sensors signals  $A$  over the interval  $[t_0 - \Delta_{input}, t_0]$ , the goal is to reconstruct a related set of signals  $B$  over the *same* interval.
- **Autoregressive (AR) Forecasting.** Given sensors signals  $A$  over  $[t_0 - \Delta_{input}, t_0]$  together with actuator trajectories over  $[t_0 - \Delta_{input}, t_0 + \Delta_{output}]$ , predict future values of the same signal set over  $[t_0, t_0 + \Delta_{output}]$ .

- **Reconstructive (RC) Forecasting.** Using sensors signals  $A$  over  $[t_0 - \Delta_{input}, t_0]$  and actuators over  $[t_0 - \Delta_{input}, t_0 + \Delta_{output}]$ , forecast a set of related outputs  $B$  over  $[t_0, t_0 + \Delta_{output}]$  where  $B$  may contain signals as in  $A$ .

We further distinguish tasks by their temporal dependency structure: **Markovian** tasks require only a short input window to make forecasts, reflecting fast dynamics, whereas **Non-Markovian (NM)** tasks require substantially longer input histories. The latter arise in phenomena governed by slower transport processes or evolving stability conditions, where even short-term predictions depend on extended plasma context.

Finally, TOKAMARK emphasizes *self-supervised* and *weakly supervised* task formulations whenever possible, reducing reliance on expert-labeled targets. This design was taken to encourage the development of AI models capable of discovering transferable plasma representations.

## 2.3 Data-driven Challenges

To complete the description of the FAIR-MAST dataset we highlight three core data-centric challenges that AI systems must overcome in order to resolve tasks in TOKAMARK. These challenges arise directly from the heterogeneous, multi-instrument nature of tokamak diagnostics and the realities of operating large fusion experiments.

- **Multi-fidelity.** Diagnostic systems operate at widely varying sampling rates, ranging from a few hundred hertz to several hundred kilohertz. Resampling to a common high-frequency time base is computationally expensive and often unnecessary, while down-sampling to the lowest frequency discards information critical for resolving fast plasma phenomena. Effective models must therefore integrate and represent multi-rate temporal data without losing fidelity.
- **Multi-modality.** Signals differ not only in physical meaning, units, numerical ranges, but also in structural forms of the corresponding data tensors. The dimensionality of the latter can be from 1 to 3 with the number of channel in each non-temporal dimension vary from 1 up to 170. AI systems must be able to fuse these diverse modalities into coherent representations suitable for downstream tasks.

- **Missing data.** As with any experimental dataset, missing information is common. Entire signals may be absent for a given shot due to hardware issues. Individual signals may also contain missing time segments, for example due to limited acquisition windows or diagnostic failures. Naively discarding shots or windows with missing components wastes valuable examples and can introduce distributional bias. Robust approaches must therefore handle incomplete signals and irregular temporal coverage in a principled manner.

### 3 MAST Benchmark

In this section, we provide a description of the main components of TOKAMARK: tasks, data preparation and evaluation protocol.

#### 3.1 Downstream Tasks

For the TOKAMARK we constructed a suite of 14 tasks designed to evaluate the core capabilities expected of AI models for real-world fusion experiments: learning unified representations from heterogeneous diagnostics, temporal reasoning across both fast and slow dynamics, robustness to incomplete state information, and generalisation across operating regimes. Those tasks span across diverse timescales, modalities, and predictive objectives.

We arranged the tasks into 4 broad groups that represent some of the major modeling challenges an AI system must master: instantaneous reconstruction, short-term magnetics dynamics, slow transport-driven profile evolution, and long-range forecasting of rare but safety-critical events and MHD activity. Table 2 summarizes definitions of tasks and groups.

**3.1.1 Group 1: Equilibrium Reconstruction.** The tasks in group 1 define a suite of reconstruction problems where the objective is to infer plasma equilibrium – its shape, boundaries, and various properties – from instantaneous magnetic measurements. The targets of the three tasks in this group span multiple modalities from scalar parameters (*task\_1-1*) to full plasma contour (*task\_1-2*) and two-dimensional representations of the poloidal magnetic flux (*task\_1-3*). The inputs of the tasks are identical and use standard magnetic diagnostics and actuator currents.

Equilibrium reconstruction is a foundational operation in tokamak experiments, performed routinely after every plasma discharge and forming the basis of essentially all downstream analysis. Traditionally, equilibrium is reconstructed by solving an inverse boundary-value problem governed by the Grad–Shafranov equation that describes the balance of magnetohydrodynamic force in axisymmetric tokamak plasmas. These solvers require multiple iterations for convergence and rely on parameterized assumptions about plasma profiles, making it challenging to deploy them in real time.

Group 1 tasks evaluate whether AI models can infer equilibrium structure directly from raw diagnostics, providing fast, numerics-free surrogates for a core analysis task that could underpin both offline interpretation and real-time control applications.

**3.1.2 Group 2: Magnetics Dynamics.** The tasks in Group 2 address short-timescale forecasting of magnetic signals, coil currents, and equilibrium evolution in response to applied actuator commands. Conceptually, these tasks parallel those in Group 1, but shift from

static reconstruction to sequence-to-sequence forecasting with actuators signals now playing an essential role in the tasks inputs. Complexity increases in the three tasks in the group: from forecasting scalar quantities – such as plasma current evolution – to joint prediction of 2D equilibrium geometry over short horizons.

At these timescales, plasma evolution is dominated by inductive coupling between active coils, passive conducting structures, and the plasma current, together with the local response of the equilibrium to perturbations. These dynamics govern how the plasma reacts to control actions during a discharge and are central to plasma position, shape, and current control. While these effects are routinely modeled offline, a model capable of achieving real time latency would enable improved control policies.

Group 2 probes whether models can learn the effective plasma-machine response encoded in coupled circuit dynamics and plasma response. This would directly target capabilities required for closed-loop control, scenario planning, and digital twin applications.

**3.1.3 Group 3: Profile Dynamics.** Group 3 tasks focus on modeling the temporal evolution of kinetic profiles – primarily electron density and temperature – and on forecasting diagnostic signals associated with confinement-mode transitions. The three tasks in this group include short-horizon forecasting (*task\_3-1* and *task\_3-2*) and pseudo-real-time reconstruction using partial, multi-rate diagnostic inputs (*task\_3-3*).

Profile evolution is governed by transport physics acting on particle and energy balance, introducing slower characteristic timescales and intrinsic memory effects compared to magnetic dynamics. These processes control energy confinement and overall plasma performance and are central to understanding transport, optimising heating schemes, and predicting access to high-performance regimes. In practice, profile measurements are often sparse, delayed, or unavailable in real time.

The main goal of Group 3 tasks is to assess AI models ability to integrate incomplete diagnostic information over time to infer latent plasma state variables. This would support applications ranging from post-shot analysis, to integrated scenario design and real-time performance monitoring and control.

**3.1.4 Group 4: MHD activity.** Finally, the tasks in Group 4 comprise long-horizon forecasting of thermal quenches (*task\_4-1* and *task\_4-2*), vertical displacement events (*task\_4-3*), current quenches (*task\_4-4*) and MHD activity leading to Locked Modes (*task\_4-5*). These tasks are focused on early detection of plasma instability and disruptions precursors that emerge across multiple diagnostic modalities. These tasks require processing of rich, high frequency inputs – including magnetics, radiative diagnostics, and time–frequency MHD signatures – over extended temporal windows, exceeding well beyond immediate system response times.

The onset of MHD instabilities and disruptions is tightly linked to the evolving equilibrium and current distribution, even when the nonlinear dynamics of the instability itself are difficult to model explicitly. Disruption avoidance and mitigation are critical operational requirements for present-day tokamaks and future reactors, directly affecting machine protection. In practice, early-warning systems rely on detecting subtle precursors distributed across multiple diagnostics and evolving over extended time windows.

**Table 2: Summary of groups and tasks for TOKAMARK.**

	Task	Input Sensors	Input Actuators	Outputs	Type	Input Window	Output Window
Group 1	1-1	Magnetics, Currents	–	Shape parameters, $\beta$ metrics	Reconstruction	5 ms	5 ms
	1-2	Same as 1-1	–	Plasma boundary	Reconstruction	5 ms	5 ms
	1-3	Same as 1-1	–	Flux map	Reconstruction	5 ms	5 ms
Group 2	2-1	Magnetics, Currents	Voltages, NBI Power	Currents, $\beta$ metrics, Shape parameters	RC Forecasting	5 ms	25 ms
	2-2	Same as 2-1	Same as 2-1	Plasma boundary	RC Forecasting	5 ms	25 ms
	2-3	Same as 2-1	Same as 2-1	Flux map	RC Forecasting	5 ms	25 ms
Group 3	3-1	Thomson scattering	References, Fueling	Thomson scattering	AR Forecasting	5 ms	50 ms
	3-2	Thomson scattering, Radiatives	Same as 3-1	Radiatives	AR Forecasting	5 ms	50 ms
	3-3	Magnetics, Currents, Interferometer	Same as 3-1	Thomson scattering, $\beta$ metrics	RC Forecasting, NM	history	5 ms
Group 4	4-1	Magnetics, Mirnov coils, Currents, Radiatives, interferometer	References, Fueling	Soft X-ray	AR Forecasting, NM	history	100 ms
	4-2	Magnetics, Mirnov coils, Currents, Radiatives, Kinetics	Same as 4-1	Soft X-ray	AR Forecasting, NM	history	100 ms
	4-3	Same as 4-1	Same as 4-1	Shape parameters	RC Forecasting, NM	history	100 ms
	4-4	Same as 4-1	Same as 4-1	Plasma current	AR Forecasting, NM	history	100 ms
	4-5	Same as 4-1	Same as 4-1	Mirnov diagnostics	AR Forecasting, NM	history	100 ms

Group 4 tasks probe models abilities to integrate long-range temporal context and multi-modal information to anticipate loss-of-control events, testing capabilities that are essential for safe and reliable fusion operation.

### 3.2 Data Preparation

From the FAIR-MAST dataset we take all 11,573 available shots and extract the data for 39 signals required by our task definitions. Before being used for model training and evaluation, these signals undergo through a standardized preprocessing pipeline to ensure consistent formatting and alignment.

**Data split.** The benchmark dataset is divided into disjoint *training*, *validation*, and *test* subsets. To avoid information leakage across sets, the split is performed at the shot level representing independent experiments and employs random sampling technique. The split ratio is 80% / 10% / 10%, and all hyperparameter tuning is conducted exclusively on the training and validation sets. The test set is held out and used only for the final performance evaluation.

**Window segmentation.** Shot-level signals data is segmented into multiple input and output windows. The lengths of those windows are task dependent and specified in Table 2. Windows are extracted using a sliding-window approach with a stride of 0.001 seconds between consecutive windows. Each input window is paired with its corresponding output window and treated as an independent window-level sample. We note that signals are used at their original sampling rates, and no resampling or imputation is performed.

**Handling missing information.** We impose additional constraints on the test set to ensure meaningful evaluation. Windows in which all input signals are entirely absent or composed solely of NaN values are excluded. Moreover, all output signals must be fully available over the entire prediction horizon.

### 3.3 Benchmark Evaluation

As part of the TOKAMARK, we introduce a hierarchical evaluation protocol for assessing model performance in a manner that aligns with scientific objectives and the structure of FAIR-MAST data. The design explicitly separates three levels of the hierarchy: (i) signals (individual physical quantities), and (ii) tasks (well-defined scientific goals), and (iii) groups (broader physical objectives). This ensures that the benchmark assess both low-level prediction quality and high-level scientific utility. For low-level evaluation, the hierarchy provides granular signal-level insights that help diagnose which physics regimes the model captures or fails to capture. For models trained jointly across multiple tasks, the same hierarchy provides modular evaluations that highlight generality and transfer properties across tasks.

To respect the hierarchy, the evaluation aggregates errors according to the following progression:

$$\text{samples} \rightarrow \text{windows} \rightarrow \text{signals} \rightarrow \text{tasks} \rightarrow \text{shots}.$$

**Samples** are the atomic level of data. For a given task and shot, each data sample is denoted as  $y_{k,i,j}$  and corresponds to a particular sample  $j$  of the flattened data from window  $i$  and signal  $k$ . In the following,  $y_{k,i,j}$  denotes the ground truth value and  $\hat{y}_{k,i,j}$  the corresponding model prediction.

**Windows** are containers of the equal per signal size storing  $N_k$  samples. We compute a window-level Root-Mean-Square error (RMSE) error as:

$$\text{RMSE}_{k,i} = \sqrt{\frac{1}{N_k} \sum_{j=1}^{N_k} (y_{k,i,j} - \hat{y}_{k,i,j})^2} \quad (1)$$

**Signals** serve as first level of the evaluation hierarchy. For each signal  $k$  containing  $M_k$  windows, we aggregate all window errors via the signal-level RMSE and normalize it with the empirical standard deviation  $\sigma_k$  computed for signal  $k$  across all evaluation shots:

$$\text{RMSE}_k = \sqrt{\frac{1}{M_k} \sum_{i=1}^{M_k} \text{RMSE}_{k,i}^2}, \quad \text{NRMSE}_k = \frac{\text{RMSE}_k}{\sigma_k} \quad (2)$$

This yields a dimensionless quantity that expresses prediction error relative to the natural variability of the target making the metric comparable across signals. An error of  $\text{NRMSE}_k = 1$  corresponds to a model no better than approximating the signal by its mean, while  $\text{NRMSE}_k < 1$  indicates predictive value. We also note that  $\text{RMSE}_k$  and  $\text{NRMSE}_k$  are computed for a given task and shot.

**Tasks.** Task-level errors  $\tilde{e}_t$  combine  $K_t$  normalized output signal errors into a single score using a uniform mean, allowing one to quantify model performance on the scientific objective as a whole:

$$\tilde{e}_t = \frac{1}{K_t} \sum_{k=1}^{K_t} \text{NRMSE}_k. \quad (3)$$

**Shots** are the final step of the aggregation sequence. They represent distinct plasma discharges and therefore provide natural boundaries for independent experimental realizations. We report per-signal and per-task shot-level averaged scores correspondingly defined as

$$\text{SignalScore} = \frac{1}{S} \sum_{s=1}^S \text{NRMSE}_{s,k}, \quad \text{TaskScore} = \frac{1}{S} \sum_{s=1}^S \tilde{e}_{s,t} \quad (4)$$

Here,  $S$  is the total number of shots in the test set used for evaluation. Finally, the group level score is taken as an average of the corresponding task scores.

## 4 Baseline Model Experiments

The baseline model is a multi-branch convolutional architecture designed to handle heterogeneous spatio-temporal inputs and outputs with varying dimensionalities (see Figure 2). Each input modality is processed by a dedicated encoder [7], and each target variable is generated by a corresponding decoder, all connected through a shared latent representation.

### 4.1 Model Description

**Encoders.** For each input variable  $v_i \in (L_t^{(0,v_i)} \times L_h^{(0,v_i)} \times L_w^{(0,v_i)})$ , an independent convolutional encoder is instantiated according to its modality: 1D convolutions for time series, 2D convolutions for profiles, and 3D convolutions for videos signals. Each encoder consists of a stack of  $N$  convolutional layers with kernel size  $K$ , stride  $s$ , and padding  $p$ , followed by ReLU activations, max-pooling, and batch normalization. The feature maps are then flattened into a latent vector. The size of the feature map  $L_d^{(t,v_i)}$  along dimension

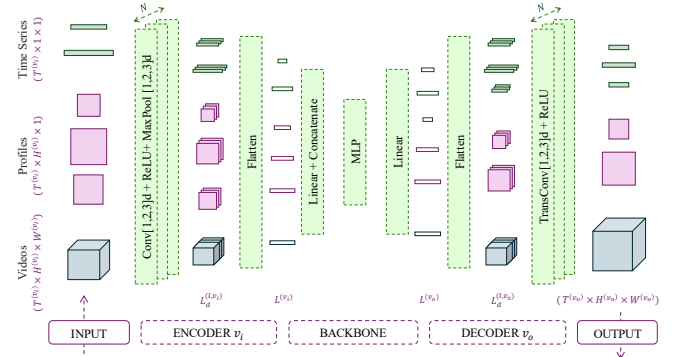


**Figure 2: Multi-branch convolutional encoder-decoder**

$d \in (t, h, w)$  after encoder layer  $\ell \in [1, N]$  and the flattened latent representation size  $L^{(v_i)}$  for variable  $v_i$  can be computed as follows:

$$L_d^{(\ell,v_i)} = \left\lfloor \frac{1}{2} \left\lfloor \frac{L_d^{(\ell-1,v_i)} + 2p - K}{s} \right\rfloor + p - \frac{1}{2} \right\rfloor + 1 \quad (5)$$

$$L^{(v_i)} = 2^{N-1} D L_t^{(N,v_i)} L_h^{(N,v_i)} L_w^{(N,v_i)} \quad (6)$$

**Latent fusion backbone.** The latent embeddings produced by all encoder branches are concatenated and passed through a shared backbone. This backbone consists of a sequence of linear layers each followed by ReLU activation and dropout, progressively reducing the dimensionality back to  $D$ . This shared representation provides a compact summary of all input data and connects the encoders and decoders blocks.

**Decoders.** For each output variable  $v_o \in (L_t^{(N,v_o)} \times L_h^{(N,v_o)} \times L_w^{(N,v_o)})$ , the decoder branch reconstructs the target output from the latent vector, mirroring the encoder structure. The shared latent vector is first reshaped into a compressed feature map of dimensionality  $L^{(v_o)}$ , which is then progressively upsampled using transposed convolutions with the output padding  $o_p$ . Cropping operations are applied after each transposed convolution to ensure that the reconstructed outputs exactly match the required target dimensions  $L_d^{(\ell,v_o)}$ . The sizes  $L_d^{(\ell,v_o)}$  of the feature map before decoder layer  $\ell \in [0, N-1]$  and  $L^{(v_o)}$  of the compressed flattened feature map are:

$$L_d^{(\ell,v_o)} = \left\lceil s \cdot (L_d^{(\ell+1,v_o)} - 1) - 2p + K + o_p \right\rceil \quad (7)$$

$$L^{(v_o)} = 2^{N-1} D L_t^{(0,v_o)} L_h^{(0,v_o)} L_w^{(0,v_o)} \quad (8)$$

### 4.2 Experimental Settings

**Parameter Settings.** For our architecture, we adopt a latent embedding dimension of  $D = 16$ , with  $N = 3$  convolutional layers per encoder and decoder blocks. Each convolution uses a kernel size  $K = 3$ , stride  $s = 3$ , padding  $p = 1$  and output padding  $o_p = 1$ . The same architectural hyperparameters – number of layers, kernel size, stride, and padding – are applied consistently across all tasks, establishing a unified baseline for the benchmark.

**Data Preprocessing.** We run a set of model specific preprocessing steps: first, we replace NaN values with zeros, second, we standardize data using signal-computed zero mean and unit variance scaler. This ensures numerical stability and helps to improve convergence during training. The training and validation data is

down-sampled by taking window samples with a stride of 0.005 seconds for Markovian tasks and 0.025 seconds for non-Markovian tasks. Furthermore, because our architecture requires a fixed-length context, all input windows are truncated to a duration of 50 ms for non-Markovian tasks.

**Training Procedure.** We train our model on mini-batches containing data from 32 shots using the Adam optimizer with a learning rate of  $1 \times 10^{-4}$  and early stopping with a patience of 10 epochs which terminates training if the validation loss does not improve over this period to prevent overfitting. We also employ a multi-output mean squared error loss, which averages the loss across all outputs of the model. Table 3 summarizes the size of models per task, computed from the encoder and decoder feature maps.

### 4.3 Experimental Results

The results of the baseline models evaluation on TOKAMARK tasks are presented in Table 3 containing task level scores and group averages. Those results demonstrate a clear distinction between tasks complexities: the model performs well for equilibrium reconstruction (Group 1) and magnetics dynamics (Group 2) tasks with group-level scores below 0.17 but degrades for profile dynamics (Group 3) and MHD activites (Group 4) tasks confirming that, as expected, these are more difficult tasks. Notably, even within the same group tasks scores vary substantially. For instance, plasma boundary reconstruction and forecasting tasks 1-2 and 2-2 are resolved much better then their counterparts within the respective groups. On the other side, the error score for task 4-5 is by far the worst and exceeds unity, suggesting the corresponding signals are poorly constrained or inadequately represented.

These results should be interpreted with a consideration to the nature of a baseline model: the architecture is generic, without physics-informed priors or task-specific tuning. The scores reported – especially those for profile dynamics and MHD activities tasks – highlight intrinsic benchmark difficulty rather than flaws in optimization. This baseline establishes a realistic lower bound and identifies areas for improvement, such as physics-aware modeling, task-adaptive weighting, or specialized architectures that should be considered by the users of TOKAMARK.

### 5 Conclusions

In this work, we introduced TOKAMARK, the first large-scale, open benchmark specifically designed for evaluating AI models on MAST tokamak diagnostics. We provided a complete open-source training and evaluation stack for 14 diverse downstream tasks together with a strong baseline model, creating an integrated framework for benchmarking, tooling, and model development.

TOKAMARK opens the door to more systematic and reproducible research in fusion plasma modeling. It provides a platform for exploring advanced representation learning of plasma, short- and long-horizon predictions, and generalization across tokamak operating regimes. We believe the adoption of TOKAMARK will accelerate progress toward practical, data-driven fusion models, foster stronger collaboration between the fusion and machine learning communities, and ultimately contribute to the development of stable and commercially viable fusion energy.

**Table 3: TaskScore and GroupScore for TOKAMARK.**

Task	TaskScore	Model size (M)
Task 1-1	<b>0.1882</b>	0.343
Task 1-2	<b>0.0482</b>	0.239
Task 1-3	<b>0.2552</b>	0.257
<i>Group 1 Score</i>	<b>0.1656</b>	–
Task 2-1	<b>0.1551</b>	0.436
Task 2-2	<b>0.0517</b>	0.277
Task 2-3	<b>0.1724</b>	0.295
<i>Group 2 Score</i>	<b>0.1290</b>	–
Task 3-1	<b>0.3252</b>	0.158
Task 3-2	<b>0.3309</b>	0.761
Task 3-3	<b>0.3607</b>	0.336
<i>Group 3 Score</i>	<b>0.3380</b>	–
Task 4-1	<b>0.3445</b>	1.518
Task 4-2	<b>0.3311</b>	1.571
Task 4-3	<b>0.2702</b>	0.672
Task 4-4	<b>0.4292</b>	0.687
Task 4-5	<b>1.0053</b>	4.741
<i>Group 4 Score</i>	<b>0.4217</b>	–

### References

- [1] R Michael Churchill. 2025. AI foundation models for experimental fusion tasks. *Frontiers in Physics* 12 (2025), 1531334.
- [2] GF Counsell, RJ Akers, Lynton C Appel, D Applegate, KB Axon, Y Baranov, C Brickley, C Bunting, RJ Butterly, PG Carolan, et al. 2005. Overview of MAST results. *Nuclear fusion* 45, 10 (2005), S157.
- [3] AJH Donné, M Cox, N Sauthoff, and K Schoenberg. 2025. Beyond power gain: Toward a comprehensive milestone framework for all fusion energy concepts. *Physics of Plasmas* 32, 9 (2025).
- [4] Samuel Jackson, Saiful Khan, Nathan Cummings, James Hodson, Shaun de Witt, Stanislas Pamela, Rob Akers, and Jeyan Thiyyagalingam. 2025. An Open Data Service for Supporting Research in Machine Learning on Tokamak Data. *IEEE Transactions on Plasma Science* (2025). doi:10.1109/TPS.2025.3583419
- [5] Samuel Jackson, Saiful Khan, Nathan Cummings, James Hodson, Shaun de Witt, Stanislas Pamela, Rob Akers, Jeyan Thiyyagalingam, and The MAST Team. 2024. FAIR-MAST: A fusion device data management system. *SoftwareX* 27 (2024), 101869.
- [6] Hendrik Meyer, RJ Akers, F Alladio, Lynton C Appel, KB Axon, N Ben Ayed, P Boerner, RJ Butterly, PG Carolan, D Cirim, et al. 2009. Overview of physics results from MAST. *Nuclear fusion* 49, 10 (2009), 104017.
- [7] Jaemin Seo, Rory Conlin, Andrew Rothstein, SangKyeun Kim, Joseph Abbate, Azarakhs Jalalvand, and Egemen Kolemen. 2023. Multimodal prediction of tearing instabilities in a tokamak. In *2023 International Joint Conference on Neural Networks (IJCNN)*. IEEE, 1–8.
- [8] Jaemin Seo, SangKyeun Kim, Azarakhs Jalalvand, Rory Conlin, Andrew Rothstein, Joseph Abbate, Keith Erickson, Josiah Wai, Ricardo Shousha, and Egemen Kolemen. 2024. Avoiding fusion plasma tearing instability with deep reinforcement learning. *Nature* 626, 8000 (2024), 746–751.
- [9] P Strand, DP Coster, M Plociennik, S de Witt, IA Klampanos, J Decker, F Imbeaux, JF Artaud, B Bosak, N Cummings, et al. 2022. A FAIR based approach to data sharing in Europe. *Plasma Physics and Controlled Fusion* 64, 10 (2022), 104001.
- [10] A Sykes, RJ Akers, LC Appel, ER Arends, PG Carolan, NJ Conway, GF Counsell, G Cunningham, A Dnestrovskij, Yu N Dnestrovskij, et al. 2001. First results from MAST. *Nuclear Fusion* 41, 10 (2001), 1423.

**Table 4: Signals taxonomy for TokAMARK.**

Category	Subcategory/Signals	Full signal name
Magnetics	Flux loops	magnetics-flux_loop_flux
	Pickup coils	magnetics-[b_field_pol_probe_ccbv_field, b_field_pol_probe_obb_field, b_field_pol_probe_obb_field]
	Saddle coils	magnetics-b_field_tor_probe_saddle_voltage
Kinetics	Thomson scattering	thomson_scattering-[t_e, n_e]
	Interferometer	interferometer-n_e_line
Radiatives	Dalpha	spectrometer_visible-filter_spectrometer_dalpha_voltage
	soft X-ray	soft_x_rays-[horizontal_cam_lower, horizontal_cam_upper]
MHD Precursors	Mirnov coils	magnetics-[b_field_tor_probe_cc_field, b_field_pol_probe_omv_voltage]
Currents	Poloidal Field Coil currents	pf_active-[coil_current, solenoid_current]
	Plasma current	summary-ip
Voltages	Poloidal Field Coil voltages	pf_active-coil_voltage
References	Reference Plasma Current	pulse_schedule-i_plasma
	Reference Plasma Density	pulse_schedule-n_e_line
Fueling	NBI power	summary-power_nbi
	Gas puffing	gas_injection-total_injected
Equilibrium	Shape parameters	equilibrium-[elongation, elongation_axis, triangularity_upper, triangularity_lower, x_point_r, x_point_z, minor_radius, magnetic_axis_r, magnetic_axis_z]
	$\beta$ metrics	equilibrium-[q95, beta_tor, beta_pol, beta_normal, bvac_rmag, bphi_rmag]
	plasma boundary	equilibrium-[lcfs_r, lcfs_z]
	flux map	equilibrium-psi

**Table 5: Group 1 detailed results.**

Task	Feature	NRMSE	NMAE
1-1	equilibrium-beta_normal	0.2734	0.1976
1-1	equilibrium-beta_pol	0.2668	0.1868
1-1	equilibrium-beta_tor	0.2415	0.1876
1-1	equilibrium-bphi_rmag	0.1497	0.1281
1-1	equilibrium-bvac_rmag	0.1367	0.1270
1-1	equilibrium-elongation	0.2342	0.1936
1-1	equilibrium-elongation_axis	0.2676	0.2240
1-1	equilibrium-magnetic_axis_r	0.1557	0.1237
1-1	equilibrium-magnetic_axis_z	0.1429	0.1173
1-1	equilibrium-minor_radius	0.1805	0.1437
1-1	equilibrium-q95	0.1749	0.1390
1-1	equilibrium-triangularity_lower	0.2277	0.1851
1-1	equilibrium-triangularity_upper	0.2155	0.1744
1-1	equilibrium-x_point_r	0.1431	0.1041
1-1	equilibrium-x_point_z	0.0130	0.0084
1-2	equilibrium-lcfs_r	0.0559	0.0390
1-2	equilibrium-lcfs_z	0.0404	0.0303
1-3	equilibrium-psi	0.2552	0.0901

**Table 6: Group 2 detailed results.**

Task	Feature	NRMSE	NMAE
2-1	equilibrium-beta_normal	0.2301	0.1639
2-1	equilibrium-beta_pol	0.2252	0.1562
2-1	equilibrium-beta_tor	0.2158	0.1647
2-1	equilibrium-bphi_rmag	0.1152	0.0911
2-1	equilibrium-bvac_rmag	0.1079	0.0969
2-1	equilibrium-elongation	0.2147	0.1742
2-1	equilibrium-elongation_axis	0.2527	0.2090
2-1	equilibrium-magnetic_axis_r	0.1462	0.1155
2-1	equilibrium-magnetic_axis_z	0.1393	0.1080
2-1	equilibrium-minor_radius	0.1677	0.1324
2-1	equilibrium-q95	0.1514	0.1220
2-1	equilibrium-triangularity_lower	0.2187	0.1734
2-1	equilibrium-triangularity_upper	0.2093	0.1641
2-1	equilibrium-x_point_r	0.1272	0.0854
2-1	equilibrium-x_point_z	0.0122	0.0078
2-1	pf_active-coil_current	0.1057	0.0739
2-1	pf_active-solenoid_current	0.0726	0.0595
2-1	summary-ip	0.0803	0.0660
2-2	equilibrium-lcfs_r	0.0561	0.0393
2-2	equilibrium-lcfs_z	0.0473	0.0355
2-3	equilibrium-psi	0.1724	0.0663

**Table 7: Group 3 detailed results.**

Task	Feature	NRMSE	NMAE
3-1	thomson_scattering-n_e	0.3307	0.2399
3-1	thomson_scattering-t_e	0.3196	0.2149
3-2	soft_x_rays-horizontal_cam_lower	0.2382	0.1136
3-2	soft_x_rays-horizontal_cam_upper	0.2717	0.1313
3-2	spectrometer_visible-filter_spectrometer_dalpha_voltage	0.4830	0.2726
3-3	equilibrium-beta_normal	0.3256	0.2211
3-3	equilibrium-beta_pol	0.3028	0.1926
3-3	equilibrium-beta_tor	0.2865	0.2101
3-3	thomson_scattering-n_e	0.5143	0.3984
3-3	thomson_scattering-t_e	0.3744	0.2817

**Table 8: Group 4 detailed results.**

Task	Feature	NRMSE	NMAE
4-1	soft_x_rays-horizontal_cam_lower	0.3184	0.1731
4-1	soft_x_rays-horizontal_cam_upper	0.3705	0.2077
4-2	soft_x_rays-horizontal_cam_lower	0.3215	0.1616
4-2	soft_x_rays-horizontal_cam_upper	0.3406	0.1792
4-3	equilibrium-magnetic_axis_z	0.2702	0.2341
4-4	summary-ip	0.4292	0.2816
4-5	magnetics-b_field_pol_probe_omv_voltage	0.9371	0.4014
4-5	magnetics-b_field_tor_probe_cc_field	1.0734	0.2972